THE ASTROPHYSICAL JOURNAL, 369:364–371, 1991 March 10

HIGH-RESOLUTION APERTURE SYNTHESIS OF MOLECULAR GAS IN NGC 1068

P. PLANESAS[1]
Centro Astronomico de Yebes, Apartado 148, 19080 Guadalajara, Spain

N. SCOVILLE
Radio Astronomy 105-24, California Institute of Technology, Pasadena, CA 91125

AND

S. T. MYERS[1]
Canadian Institute for Theoretical Astrophysics, McLennan Labs, University of Toronto, Toronto, Ontario, Canada M5S 1A1
Received 1990 June 1; accepted 1990 August 27

ABSTRACT

We present high-resolution (2″.9 ~ 260 pc) aperture synthesis imaging of NGC 1068 in the CO $J = 1 \rightarrow 0$ line made with the Owens Valley Millimeter Interferometer. The major features seen in CO are (1) the inner spiral arms of molecular gas at ~15″ radius (1.5 kpc) which originate from the ends of the central stellar bar, and (2) a compact source (~3″) coincident with the Seyfert 2 nucleus. These components within 2 kpc of the galactic nucleus account for approximately 30% of the total molecular gas content in NGC 1068. The spiral arm CO emission is resolved into 38 discrete complexes which closely correlate with regions of strong Hα and 10 μm emission. The sizes of these structures range up to 500 pc and their masses derived from the CO line flux are (2×10^7)–(7×10^8) $M_\odot$. Somewhat smaller mass estimates are obtained from the virial theorem using the observed CO line widths and sizes, suggesting that these complexes may be self-gravitating.

Radio continuum emission from the nucleus was detected at both 112 and 115 GHz. The flux density measured in the upper sideband (centered on the CO line) is significantly larger than the nonthermal radio continuum measured in the lower sideband. Assuming that this excess is CO line emission, then the derived H_2 mass for the central source is 8×10^7 $M_\odot$ (within 130 pc radius). The inferred column densities of neutral gas and dust are consistent with those inferred for the dusty torus hypothesized to obscure a Seyfert 1 nucleus. It is suggested that the stellar bar in the inner disk provides a common link between the spiral arm starbursts, the centimeter-wave radio jets, and the active nucleus phenomena through dynamical effects on the dense molecular gas.

Subject headings: galaxies: individual (NGC 1068) — galaxies: interstellar matter — galaxies: Seyfert — galaxies: structure

1. INTRODUCTION

In recent years, it has become apparent that star formation in the central regions of "starburst" galaxies may be linked to the formation and fueling of an active galactic nucleus (AGN) as found in Seyfert galaxies and quasars (cf. Norman & Scoville 1988; Sanders et al. 1988). Analysis of the IRAS survey indicated that ~50% of galaxies with 60 μm luminosities above 10^{11} $L_\odot$ show optical line ratios signifying the presence of nonthermal power-law excitation in the UV, while at lower luminosities, the majority of the galaxies exhibit line ratios suggestive of OB star ionization (Sanders et al. 1988). The starburst and AGN phenomena could be promoted by an abundant supply of interstellar gas which would both sustain a high rate of star formation and feed a central black hole. Because the lifetimes of these phenomena are short and they are seen in otherwise old galaxies, it is unlikely that such activity is produced as a normal, albeit transient, phase in the life cycle of a normal, isolated galaxy.

Perturbative mechanisms such as galaxy-galaxy interactions and mergers can provide both the fuel and the mechanism for transporting the gas to the center of the host galaxy. This increased frequency of AGNs and starbursts in interacting galaxy systems has been pointed out by Dahari (1984, 1985), Hutchings & Campbell (1983), and Bushouse (1987). Numerical simulations of such interactions show that dissipative effects in the gas can promote the transfer of interstellar matter into the nuclei of the colliding galaxies (Hernquist 1989). In a more controlled and gradual way, the nonaxisymmetric gravitational potential of a central stellar bar, perhaps formed during a close encounter, will induce noncircular motions which increase the effective viscosity of the ISM and hence, raise the rate at which gas accretes to the galactic center (Noguchi 1988). However, it is clear that since a large fraction of both interacting and barred spiral galaxies show no evidence of either AGN or starburst activity, gravitational perturbation is not *sufficient* for these phenomena. The existence of an abundance gas supply is certainly necessary for the starburst and may also be necessary, at least in the early phases, of the AGN.

Studies of the kinematics of the molecular gas and young stars in these galaxies can provide clues to the nature of the triggering mechanisms of this activity as well as establish the presence of a causal link between the two. The Seyfert 2 galaxy NGC 1068 is the nearest object showing both AGN and starburst characteristics. The bolometric luminosity ($\sim 3 \times 10^{11}$ $L_\odot$) is approximately equally split between an extended inner disk of radius 1.5 kpc and a central pointlike (<30 pc) AGN source (Telesco et al. 1984). The nucleus exhibits a Seyfert 2 spectrum, but optical spectropolarimetry has revealed the presence of a broad polarized component to the narrow emission lines, indicating a possible obscured Seyfert 1 nucleus

[1] Also California Institute of Technology.

(Antonucci & Miller 1985). On arcsecond angular scales, radio continuum images show a triple source with jetlike morphology (Ulvestad, Neff, & Wilson 1987), also characteristic of AGN activity. Optical and near-infrared observations of the bright inner ($<15''$) disk indicate a young stellar spectrum with strong Balmer absorption lines and emission lines suggesting a large population of B type stars and associated H II regions, typical of a starburst (cf. Wynn-Williams, Becklin, & Scoville 1985). NGC 1068 also contains a non axisymmetric gravitational potential, with strong spiral arms and clear evidence of a central bar feature in $\lambda = 1.6$–2.2 μm continuum images, extending $\sim 30''$ across the inner disk (Scoville et al. 1988; Thronson et al. 1989). The galaxy is extraordinarily rich in molecular gas, with a total H_2 mass estimated to be 1.5×10^{10} $M_\odot$ (Scoville, Young, & Lucy 1983; Planesas, Gomez-Gonzales, and Martin-Pintado 1989). Because NGC 1068 exhibits the characteristics of an active starburst, AGN properties, and spiral and bar structure, as well as large amounts of gas, it is an ideal target for kinematic and morphological studies of the molecular cloud complexes and young stellar associations in a gas-rich environment and elucidating the links between the starburst and AGN phenomena. See Table 1.

Previous aperture synthesis observations (Myers & Scoville 1987, hereafter Paper I) indicate that a significant fraction of the gas is contained within a discontinuous ringlike structure of radius 1.6 kpc, at the outside of the inner star-forming disk. In this paper, we report new interferometric data for the 115 GHz $J = 1 \rightarrow 0$ CO line. These observations provide higher sensitivity and improved angular resolution ($2''.9$, a factor of 2–3 better than in the previous study) allowing the resolution of cloud complexes within the ring structure and the detection of a central gas concentration. We begin in § 2 with a summary of the observations and data reduction, followed by a discussion of the distribution, kinematics and properties of the CO in § 3. The emission at the nucleus is discussed in § 4.

TABLE 1

ADOPTED PARAMETERS FOR NGC 1068

Parameter	Value
α_{1950}[a]	$2^h40^m07^s.076$
δ_{1950}[a]	$-0°13'31''.45$
Inclination	40°
V_{lsr}[b]	1125 km s^{-1}
Distance[c]	18.1 Mpc
Linear size equivalent to $1''$	90 pc
L_{FIR}[d]	1.5×10^{11} $L_\odot$
H_2 mass from single-dish observations[e]	1.5×10^{10} $M_\odot$

[a] Optical nucleus position; Clements 1981.
[b] Mean velocity from single-dish CO observations.
[c] Sandage and Tammann 1981.
[d] Excluding nuclear point source.
[e] Scoville et al. 1983; Planesas et al. 1989.

2. OBSERVATIONS

Aperture synthesis observations of the CO ($J = 1$–0) line were obtained from 1988 November to 1989 March with the Owens Valley Radio Observatory (OVRO) three-element millimeter-wave interferometer. Each of the 10.4 m telescopes was equipped with an SIS receiver cooled to 4.5 K. Measured receiver temperatures were approximately 160 K SSB. Spectral coverage was provided by a filterbank consisting of 32×5 MHz channels encompassing 416 km s^{-1} at a resolution of 13 km s^{-1} in the CO line. Radio continuum measurements in both sidebands were simultaneously obtained using a 400 MHz continuum filter. NGC 1068 was observed in seven configurations with baselines out to 200 m east-west and 140 m north-south. The uniformly weighted synthesized beam was $2''.9 \times 2''.9$, corresponding to a linear size of 260 pc at a distance of 18.1 Mpc (Sandage & Tammann 1975). The field of view for the telescopes is $70''$.

Observations of the radio source (0221+067) every 20 minutes were used for phase calibration. The phase stability was extremely good during most of the tracks with typical gradients over an 8 hr period being less than 30°. Variations in the receiver gain and sky opacity were calibrated by measurement of an ambient temperature chopper wheel at the beginning of each 5 minute integration. The absolute flux density scale was established from observations of Mars ($T_B = 206$–212 K), Uranus ($T_B = 120$ K), and 3C 84 with appropriate corrections made for the expected visibilities of the planets. Passband calibration was based upon the observations of 3C 84.

The interferometer data were processed after the initial calibration using the NRAO AIPS package. Single channel and four-channel average maps were produced using the AIPS routine MX. No zero spacing flux was specified. The resulting single-channel maps had a typical rms of 60 mJy beam^{-1}, approximately a factor of 4 lower than that obtained in the previous observations (Paper I). This large increase in effective sensitivity is a result of significant improvements in receiver sensitivity, phase stability, and the aperture efficiency of the telescopes over the last 2 yr. The maps were corrected for fall-off in the primary beam response assuming a Gaussian of $70''$ FWHP. To check the consistency of the present data with the previous observations, we have generated maps convolved to $7''$ resolution. These are generally similar in structure to those presented in Paper I.

3. CO DISTRIBUTION AND KINEMATICS

In Figure 1, the CO map obtained by summing the emission from all of the 5 MHz filters is shown superposed on an optical (U-band) image of the galaxy. The dominant structure seen is the spiral arms at $10''$–$15''$ radius which encircle the bright, central optical disk. The high-resolution CO features in this structure are closely correlated with areas of reduced optical emission at the outer edge of the inner disk, presumably regions of high dust extinction. A new feature not seen in the previous low-resolution aperture synthesis is present—an unresolved emission source at the position of the optical nucleus. This region will be discussed in detail in § 4.

3.1. CO *Kinematics*

In Figure 2, the centroid velocity of the CO emission is shown in contour form superposed on an outline of the CO emission contours from Figure 1. The straight lines drawn across the center of the ring structure connect equal velocity contours on the northern and southern sides.

The CO kinematics appear extremely ordered, and we have fitted two models to the observed kinematics: one in which the line of modes position angle was constrained to be 55° (cf. Sandage 1961), the second in which the line of nodes PA was a free parameter (i.e., the *kinematic* major axis was solved for). In the first model, the circular and radial velocities were varied as a function of galactic radius; in the second model, only the circular velocity was varied and the random, noncircular velocities were estimated from the errors in the fit at each radius. In

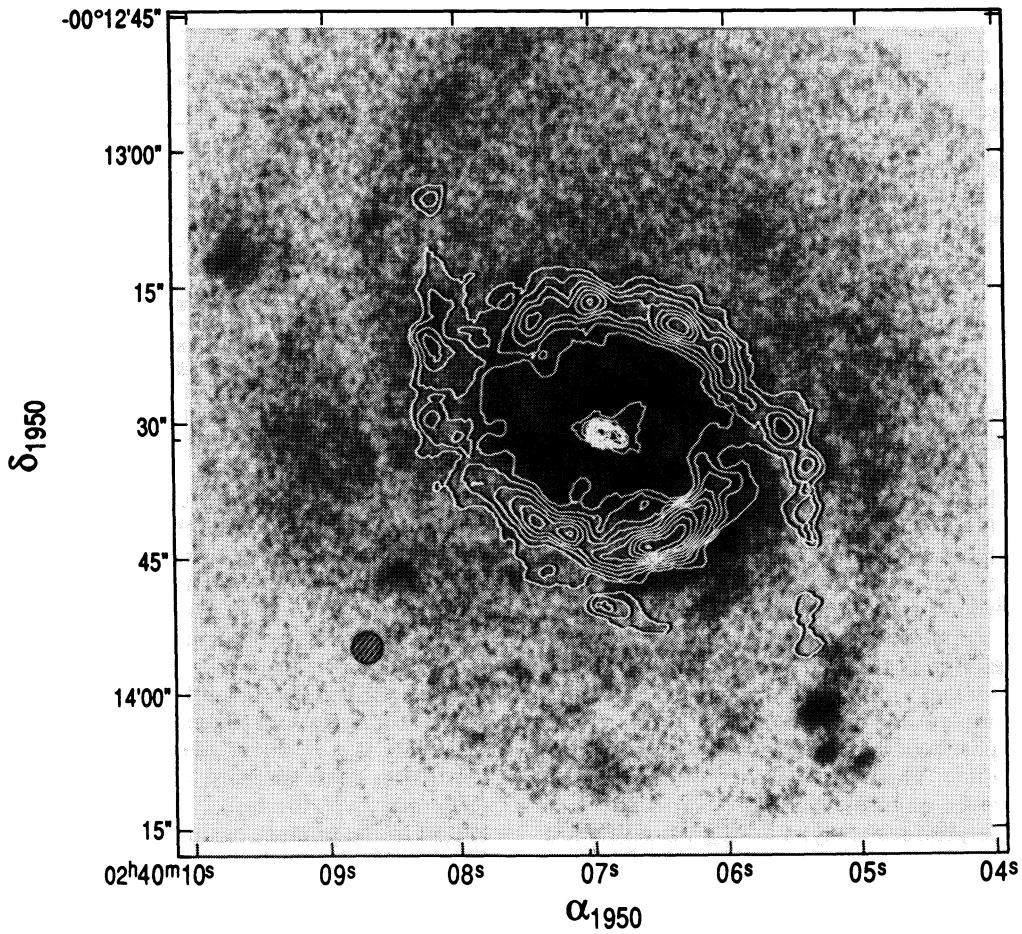

FIG. 1.—Map of the integrated CO emission in NGC 1068 overlaid on a U-band image of the inner region of the galaxy taken with the University of Hawaii 88 inch (2.3 m) telescope by B. Tully. The synthesized beam size (2".9 × 2".9) is shown in the lower left-hand corner. The contour levels are multiples of 5.2 Jy km s^{-1} $beam^{-1}$.

both models, the adopted inclination was 40°. (The emission from the nucleus [see § 4] is excluded from this fitting.) The results are summarized in Table 2. For the model with purely circular velocities, the derived position angle of the kinematic major axis is 87° ± 1°, in excellent agreement with the values derived in Paper I and Baldwin, Wilson, & Whittle (1987). For the fit involving both circular and radial motions, parameters similar to those derived Paper I were obtained, i.e., a mass-weighted mean rotation velocity of 170 km s^{-1}, an expansion velocity of 100 km s^{-1}, and a mean radius of 1.7 kpc (see Table 2).

The velocity dispersion of the CO emission in the ring varies between 13 and 50 km s^{-1}. The latter is substantially larger than that expected due to smearing of the large-scale velocity field over the area of the synthesized beam and much larger than is seen in individual Galactic GMCs (σ_v = 3–8 km s^{-1}; Scoville & Good 1989). The dispersion is particularly high in the large emission feature to the south-southwest of the nucleus (complex 20, § 3.4).

3.2. *Molecular Gas Morphology*

The overall morphology of the molecular emission can be most simply modeled as two spiral arms originating at the ends of the near-infrared bar which crosses the inner disk. In Figure 3*a*, a polar plot of the CO emission with the r, θ coordinates derived from deprojection of the observed α, δ (assuming i = 40° and P.A. = 87°.) The majority of the emission appears at constant radius, but the two arm segments in the northeast and southwest are clearly inclined with respect to this struc-

TABLE 2

DERIVED PARAMETERS FOR THE MOLECULAR RING

R (kpc)	$\langle R \rangle$ (kpc)	V_{circ} (km s^{-1})	V_{exp} (km s^{-1})	M_{H_2} (10^8 $M_\odot$)
		PA = 55°		
0.6–0.9	0.84	31	33	0.5
0.9–1.2	1.09	195	119	4.9
1.2–1.5	1.36	194	103	16.8
1.5–1.8	1.64	163	92	14.0
1.8–2.1	1.94	145	100	7.4
2.1–2.4	2.21	112	108	2.5
Weighted mean	1.65	171	100	...
		PA = 87°		
0.6–0.9	0.87	69	38	0.1
0.9–1.2	1.09	221	24	3.5
1.2–1.5	1.36	220	−11	16.2
1.5–1.8	1.65	206	−4	17.7
1.8–2.1	1.92	183	11	5.9
2.1–2.4	2.23	172	31	2.1
Weighted mean	1.74	207	−1	...

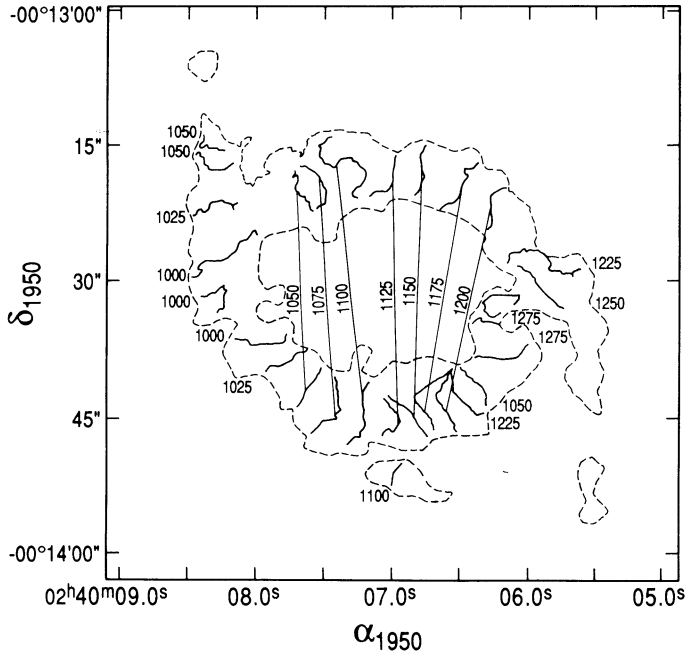

FIG. 2.—Contours of the centroid velocity for the CO emission are superposed on an outline of the CO emission. The velocity contours are labeled with the LSR velocity. The straight lines connect equal velocity contours on the northern and southern sides of the ring. The largest velocity gradients in the spiral arms occur in the large mass concentrations at the ends of the stellar bar at P.A. = 48°.

ture. The derived pitch angle for the two outer arm segments is approximately 35°. On the other hand, if line of nodes position angle of 55° is used, the polar plot in Figure 3*b* results. The emission structure *now appears much more continuous* with a constant pitch angle of 7°–10°.

Two alternative models for the CO emission are a constant radius ring with short spiral arm segments leading to the outer disk or a continuous pair of spiral arms. We favor the latter interpretation for the molecular gas morphology in view of the fact that the two major CO concentrations, northeast and southwest of the nucleus occur at the ends of the stellar bar seen at $\lambda = 2$ μm (P.A. = 45°–48°; Scoville et al. 1988 and Thronson et al. 1989). The spiral arms can then be traced continuously, trailing behind these features, with smoothly decreasing intensity in the clockwise direction. This continuity is apparent in the polar diagram (Fig. 3*b*). In this interpretation, the velocity field must therefore have significant noncircular motions, but these might plausibly arise from the nonaxisymmetric gravitational potential of the massive stellar bar at P.A. = 48° (see Fig. 4). For this geometry, the southeast disk must be on the near side of the galaxy.

3.3. *Molecular Gas Complexes*

An interesting feature of the new data is the resolution of the emission structure into discrete complexes. In the individual 5 MHz maps, we have isolated 38 complexes. The locations of these structures are noted in Figure 5 on the integrated CO intensity map and although not all of the complexes can be seen as discrete features in the integrated intensity map, most are clearly separable on the basis of the individual channel maps. The positions ($\Delta\alpha$, $\Delta\delta$ relative to the nucleus), integrated CO line fluxes, peak brightness temperatures, mean velocities, and velocity dispersions of the features are listed in Table 3. Also included in Table 3 are the molecular masses derived from the integrated CO line fluxes and the virial masses derived from the measured line widths and sizes. More than one-half of

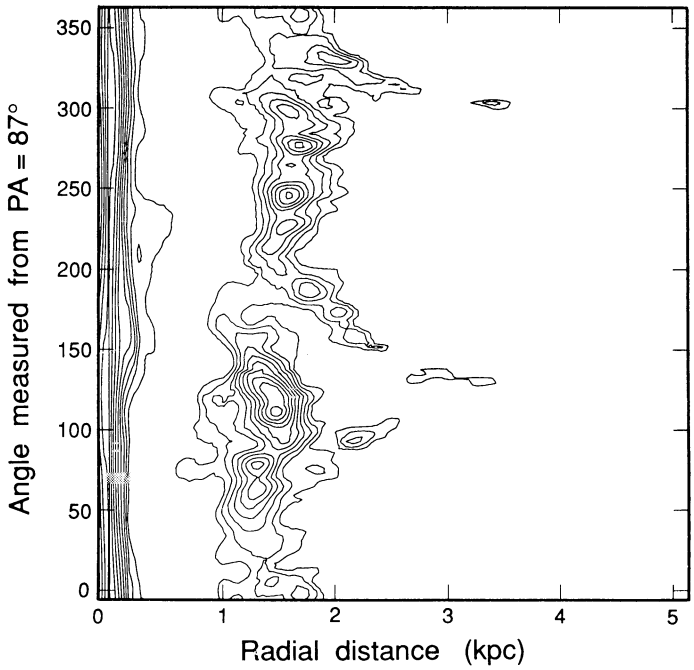

FIG. 3*a*

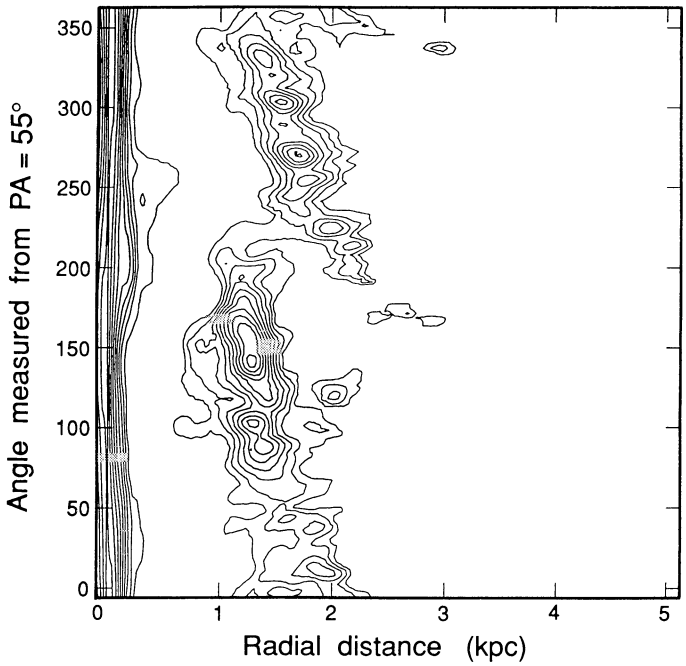

FIG. 3*b*

FIG. 3.—Polar plots of the CO emission obtained from deprojection of the observed map assuming an inclination for the disk of the galaxy of 40°. In (*a*), the position angle for the major axis was taken to be 87° (the kinematic major axis); in (*b*), the isophotal major axis P.A. = 55° is used. The average width of the spiral arms is 5″ (~450 pc).

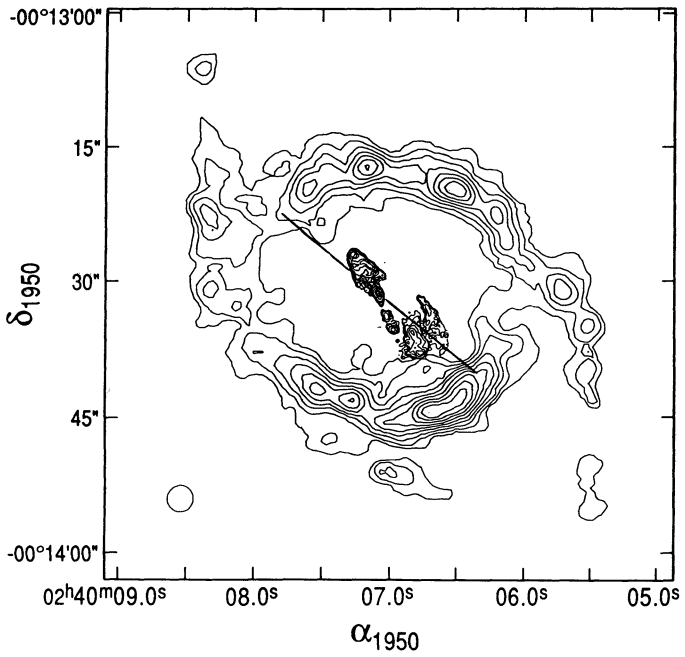

FIG. 4.—Map of the integrated CO emission in NGC 1068 overlaid on a VLA 4.9 GHz radio continuum map (Wilson & Ulvestad 1987). The emission from the nucleus at 115 GHz has been removed for clarity. The straight line across the center indicates the 2.2 μm bar orientation (Scoville et al. 1988).

the features are resolved in at least one spatial dimension, and 22 of the features have $\Delta v \geq 30$ km s^{-1}. Approximately 80% of the total flux appearing in Figure 1 is contained within the features included in Table 3.

The observed brightness temperatures of the CO complexes are in the range 2–15 K averaged over the synthesized beam

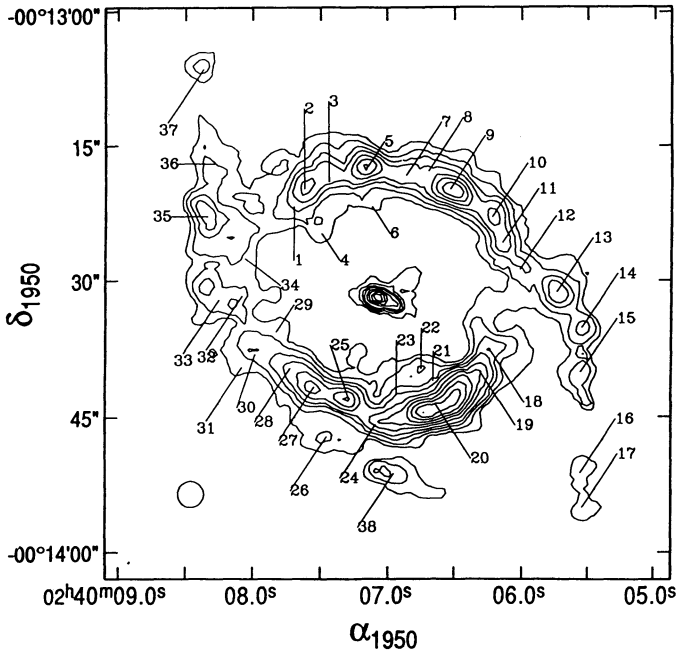

FIG. 5.—Map of the integrated CO emission in NGC 1068 with the locations of the molecular cloud complexes identified from the individual channel maps. The numbers correspond to the features listed in Table 3.

(260 pc in diameter). These brightness temperatures are substantially higher than those which would be obtained in the CO emission complexes of our Galaxy, viewed at a similar linear resolution. The molecular gas in the NGC 1068 complexes must therefore have a higher area filling factor and substantially higher excitation temperatures. The higher temperatures probably result from heating by the much stronger radiation field in the central disk of NGC 1068. Averaged over the disk of the Milky Way, the mean ratio of L_{IR}/M_{H_2} is 3 $L_\odot$ $M_\odot^{-1}$ as derived from *IRAS* and CO observations in the inner Galaxy (Scoville & Good 1989). In contrast, the central 3 kpc of NGC 1068 has a total far-infrared luminosity, excluding the nuclear source, of 1.5×10^{11} $L_\odot$ (Telesco et al. 1984) and a *total* molecular gas mass of $\lesssim 10^{10}$ $M_\odot$. Thus, the apparent ratio of L_{IR}/M_{H_2} is $\gtrsim 15$ $L_\odot$ $M_\odot^{-1}$, a factor of 5 greater than that in the Milky Way. The greater luminosity per unit gas mass in the NGC 1068 spiral arms is probably due to a greater rate of star formation and hence, a higher rate of heating by embedded stars (and by external sources).

The masses derived from the CO line flux are based upon an adopted Galactic CO-to-H_2 conversion $\alpha = 3 \times 10^{20}$ cm^{-2} (K km s^{-1})$^{-1}$ (cf. Scoville & Sanders 1987). The typical sizes of the structures range up to a maximum size of 500 pc. In all cases, these features are much larger than individual giant molecular clouds seen in our galaxy. In addition, the measured velocity dispersions are factors of 3–6 greater than those of Galactic GMCs. The masses derived from the CO line flux and from the assumption of gravitational binding are in the range (1×10^7)–(7×10^8) $M_\odot$, i.e., a factor of 100 greater than those of typical Galactic GMCs.

It is noteworthy that in most of the NGC 1068 features, the derived virial masses are typically a factor of 2 lower than the masses derived from CO line flux. This discrepancy is particularly significant in view of the fact that the observed structures may not be gravitationally bound and the virial masses would therefore have been overestimated. This discrepancy may be resolved if the CO-to-H_2 conversion factor is reduced from the Galactic value adopted here. Single-dish CO (1–0) and (2–1) observations by Planesas et al. (1989) have shown a gradient in the 2–1/1–0 ratio with radius in NGC 1068 which they interpret in terms of molecular gas being hotter and somewhat denser toward the center of the galaxy than at larger radii. This conclusion is consistent with the ^{13}CO observations of Young & Sanders (1987) which suggest significantly hotter gas in the central 55″ of NGC 1068. The Galactic GMCs for which the CO-to-H_2 conversion factor was derived have typical gas temperatures of $T_K = 5$–10 K (cf. Scoville & Sanders 1987). The CO-to-H_2 conversion ratio is expected to scale at $\bar{n}_{H_2}^{1/2}/T_K$ and thus, for gas a factor of 4 hotter in NGC 1068, the CO-to-H_2 conversion factor should be reduced to 0.25 of that in the Galactic GMCs (assuming the densities are similar). If the masses derived from the CO line flux are scaled down by this factor, the values listed in Table 3 will typically be 0.5 of the virial masses. It should be noted that since the observed brightness temperatures are already quite high, the area filling factors of the emitting clouds must be $\gtrsim 0.1$ and the assumption of a higher kinetic temperature in the NGC 1068 complexes implies a correspondingly higher mean density. These higher densities will, to some extent, offset the effects of the elevated temperatues on the CO-to-H_2 conversion factor.

The resolution of our data is insufficient to determine with certainty if the structures in NGC 1068 are gravitationally bound complexes of giant molecular clouds or are a different

TABLE 3

MOLECULAR CLOUD COMPLEXES

Number	$\Delta\alpha$[a]	$\Delta\delta$[a]	CO (Jy km s^{-1})	T_B(peak) (K)	V_{lsr} (km s^{-1})	ΔV (km s^{-1})	M_{CO} ($10^7 M_\odot$)	M_{vir} ($10^7 M_\odot$)
1.....	9".7	10".0	13	8	1023	18	5.3	1.3
2.....	8.3	12.0	26	8	1054	35	10.3	3.9
3.....	5.6	12.8	36	9	1099	43	14.1	8.5
4.....	6.4	7.0	6	3	1138	23	2.3	1.3
5.....	1.4	14.3	55	12	1108	48	21.5	8.2
6.....	0.8	10.0	5	2	1146	26	2.0	2.0
7.....	−3.1	13.5	25	12	1139	22	9.9	1.9
8.....	−5.6	14.0	13	7	1163	21	5.2	1.5
9.....	−8.1	12.0	67	14	1174	52	26.4	12.1
10.....	−12.9	8.9	36	10	1202	38	14.3	5.4
11.....	−14.1	6.0	29	9	1217	36	11.6	5.8
12.....	−16.1	3.0	14	6	1262	27	5.7	2.6
13.....	−20.3	0.5	37	8	1237	50	14.7	10.1
14.....	−23.1	−3.5	21	6	1243	39	8.2	5.2
15.....	−23.0	−8.5	19	7	1236	31	7.6	3.8
16.....	−22.9	−19.8	11	5	1207	27	4.4	3.4
17.....	−23.1	−23.7	17	5	1202	38	6.5	5.7
18.....	−12.6	−5.9	29	10	1284	30	11.3	3.4
19.....	−11.6	−8.5	38	12	1267	35	15.1	4.7
20.....	−6.5	−12.2	180	15	1184	130	71.0	...
21.....	−6.2	−9.5	9	4	1176	21	3.4	2.2
22.....	−4.8	−8.1	19	5	1142	44	7.3	7.5
23.....	−2.0	−11.0	10	3	1170	38	3.9	3.9
24.....	0.4	−14.4	6	3	1149	20	2.5	1.2
25.....	3.4	−11.5	42	10	1091	48	16.6	8.3
26.....	5.9	−15.8	18	6	1084	33	7.2	4.5
27.....	7.2	−10.2	52	11	1055	52	20.6	11.9
28.....	9.9	−8.1	27	8	1021	35	10.6	6.5
29.....	11.5	−4.0	8	7	988	13	3.3	(0.6)
30.....	13.9	−6.5	7	6	1001	13	2.6	(0.6)
31.....	15.4	−8.0	5	4	1014	13	2.0	(0.6)
32.....	15.4	0.0	8	7	988	13	3.2	(0.6)
33.....	18.0	−0.4	12	6	1008	24	4.8	2.0
34.....	15.0	4.2	10	6	984	19	3.9	1.5
35.....	19.3	8.9	33	12	1026	30	13.0	3.8
36.....	18.5	14.8	8	7	1053	13	3.1	(0.6)
37.....	19.7	25.4	13	4	1015	34	5.3	4.0
38.....	−1.6	−19.9	25	6	1102	43	9.9	7.4

[a] Offsets from nucleus ($\alpha_{1950} = 2^h40^m07^s.08$, $\delta_{1950} = -00°13'31".45$).

class of interstellar cloud. High-resolution CO interferometry of M51 by Vogel, Kulkarni, & Scoville (1988) and Rand & Kulkarni (1990) have revealed large associations of molecular clouds, most of them in the spiral dust arms. Some of these structures were found to be in virial equilibrium assuming a standard CO-to-H_2 ratio, but others were not. The structures seen by us in NGC 1068 are typically a factor of 5 more massive than those in the spiral arms of M51, but similar to those seen in the nucleus of M51.

Complexes 1–12 are located in the northern spiral arm (Fig. 5). A 10.8 μm map of roughly the same region of NGC 1068 (Telesco & Decher 1988) shows emission covering most of this area. Several peaks of IR emission can be identified in their map, all of them lay close to prominent molecular cloud complexes, namely complexes 1, 5, 7, 9, 10, and 12. The northern arm is also well delimited by a string of Hα emission regions, as can be seen, e.g., in the intensity map by Atherton et al. (1985). The arm segment defined by the complexes 13–17, however, lies in a region with very little Hα emission.

The southern arm is not well defined in the 10.8 μm and Hα maps. The emission in both cases is concentrated in the southwest. In particular, very strong and extended Hα emission is detected in a region located southwest of complexes 18–20. The 10.8 μm emission has a similar distribution, but the peak emission lies closer to the center of complex 20. At the eastern end of the southern arm, there are some of the less massive complexes. Some of them appear in only one channel, so the velocity dispersion quoted in Table 3 is, in fact, an upper limit.

It is interesting to note that the Hα velocity field has a irregular structure in the southwest region. The high angular and high velocity resolution spectrophotometry by Cecil, Bland, & Tully (1990) shows isovelocity contours parallel to the stellar bar on the inside, but curving abruptly just before reaching the largest concentration (20) of molecular gas in the southern arm. Complex 20 is the largest in size, mass (7×10^8 $M_\odot$), and velocity dispersion (it is detected over a range of 200 km s^{-1}). The emission shows a velocity gradient, but the distribution is so continuous that it is not possible to separate it into discrete components. Complex 25, 4 times smaller in mass, is also detected over 100 km s^{-1} with the peak position shifting slightly from one channel to the next.

4. NUCLEAR EMISSION

In Figures 6*a* and 6*b*, the continuum emission in the lower and upper sidebands (at 111.9 and 114.8 GHz) are shown. The

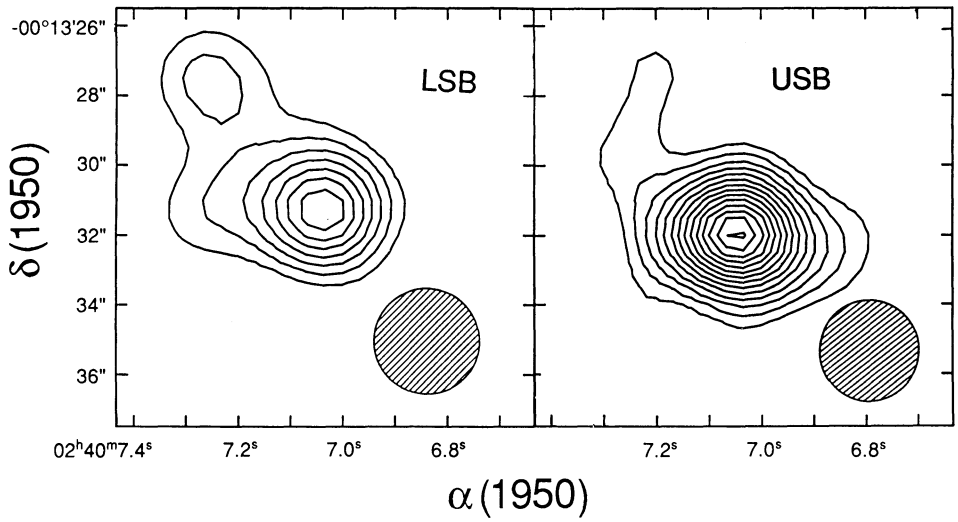

FIG. 6.—Continuum maps of the nuclear region of NGC 1068 at 111.9 (LSB) and 114.8 GHz (USB). The rms (1 σ) noise in the maps are 3.5 and 5.1 mJy beam^{-1}, respectively. The first contour corresponds to ± 7.0 mJy beam^{-1}, and the contour interval is 3.5 mJy beam^{-1}. Negative contours are shown dashed. The beam size is shown as a circle on the lower right-hand corner in each panel. The values for peak and integrated flux density are given in Table 4.

signal in the lower sideband for which the bandpass contains no known molecular features is entirely nonthermal radio continuum from the nuclear source (Wilson & Ulvestad 1982), while that in the upper sideband contains both continuum emission and CO emission across the 400 MHz (1040 km s^{-1}) bandpass. In Table 4, the flux densities are given. No significant continuum emission is detected in the lower sideband from the spiral arms.

The nuclear source at radii $< 3''$ has a peak flux density of 31 mJy beam^{-1} at 112 GHz which is consistent with the flux density and spectral index measured at 15 and 22 GHz (Ulvestad et al. 1987). The central continuum source (Fig. 6*b*) also shows a possible extension to the northeast corresponding to the position angle of the jet seen at centimeter wavelengths. In the upper sideband (Fig. 6*b*, Table 4), the central source flux density is significantly stronger (50 mJy beam^{-1}). The rms noise in the lower sideband continuum map is 3.5 mJy, and that in the upper sideband continuum map is 5.1 mJy. Thus, the excess of 19 mJy measured in the upper sideband which contains the CO line corresponds to approximately 4 σ. The excess flux in the upper sideband, attributed to CO, appears to be centered slightly south of the radio continuum *centroid* (compare Figs. 6*a* and 6*b*), i.e., near the southernmost of the three compact nuclear sources. This location coincides with the H_2O maser source (Claussen & Lo 1986). Assuming that this excess is CO emission from the nucleus, then the derived H_2 mass is $8 \times 10^7\ M_\odot$ (assuming the normal Galactic CO-to-H_2 conversion ratio). As discussed above, the derived H_2 mass could be substantially less if the gas is much hotter here (or significantly greater if the gas is much denser). If the H_2 mass derived above for the nuclear source is uniformly distributed within a sphere of diameter 260 pc, the average H_2 density is 175 cm^{-3} and a lower limit to the extinction is $A_v = 140$ mag for a standard Galactic gas-to-dust ratio. The expected continuum emission of the dust at the CO frequency is 5 mJy for dust temperatures 50 K and a mass of $8 \times 10^7\ M_\odot$.

TABLE 4

CENTRAL SOURCE RADIO CONTINUUM MEASUREMENTS

Parameter	Value
USB 114.8 GHz	
Peak intensity	50 ± 2 mJy beam^{-1}
Integral intensity	76 ± 5 mJy
Measured size	$4''.0 \times 3''.0$
RMS noise	5.1 mJy
LSB 111.9 GHz	
Central source	
Peak intensity	31 ± 1 mJy beam^{-1}
Integral intensity	33 ± 3 mJy
Measured size	$3''.2 \times 2''.9$
RMS noise	3.5 mJy
NE source	
Peak intensity	12 ± 1 mJy beam^{-1}

The detection of neutral molecular gas within 130 pc of the central AGN in NGC 1068 is particularly interesting in view of the optical spectropolarimetry showing broad emission lines which have been interpreted as an obscured Seyfert 1 nucleus seen in scattered light (Antonucci & Miller 1985). They postulated that a dusty torus surronding the Seyfert 1 nucleus blocks our direct line of sight. (It is interesting to note that Krabbe et al. 1990 have detected a torus of 2.1 μm H_2 emission entered on the radio peak with a radius of $1''.5$. The inferred H_2 mass is $10^4\ M_\odot$ for $T_{vib} = 2000$ K.) The high column densities of neutral gas and dust derived for the CO nuclear source are consistent with this hypothesis. If the molecular mass is distributed in a 70 pc diameter sphere, the extinction to the nucleus would be 10^3 mag, providing an opacity high enough to stop most of the hard X-ray emission (Kallman & Mushotzky 1985).

5. CONCLUSIONS

The major features of the molecular distribution in the central 3 kpc of NGC 1068 are a continuous pair of spiral arms originating from the end of the stellar bar seen in $\lambda = 2.2$ μm images and a nuclear gas concentration of approximately $8 \times 10^7\ M_\odot$. The total molecular gas content of the spiral arms is $5 \times 10^9\ M_\odot$; most of this gas is distributed in 38 com-

plexes of mass 10^7–7×10^8 $M_\odot$ with sizes ranging up to 500 pc. The large reservoir of interstellar gas seen in the spiral arms at 1.7 kpc radius may play a central role in both the abundant star formation and nuclear activity. The link between the spiral arms and the active nucleus could be provided by the massive stellar bar seen at $\lambda = 2$ μm (e.g., Telesco & Decher 1988). Theoretical studies of the gas orbits within a bar potential by Roberts, Huntley, & van Albada (1979), Huntley (1980), and Noguchi (1988) have shown that the orbits are highly elliptical and not strictly closed. In this situation, the gas, having a high effective viscosity, can decay rapidly inward, fueling the nuclear activity. Direct evidence that the bar exerts a significant, non-axisymmetric force on the molecular gas is provided by the CO kinematics reported here if the major axis position angle is taken to be approximately 55° (as implied by the continuity of the deprojected molecular gas spiral arms). The large velocity dispersion induced in the gas by the bar will enhance the accretion rate to the inner disk. It is of interest to note that the nonthermal radio jets seen by Wilson & Ulvestad (1983) are aligned at P.A. = 30°, i.e., approximately along the bar axis. Whether this alignment of the radio emission is related to the gravitational potential of the bar or the focusing effects of dense interstellar gas within the bar is unclear on the basis of the present observations. It is also possible that the central molecular gas concentration discovered within 130 pc of the nucleus, both obscures the central AGN and provides the collimation of the radio emission.

This research was supported in part by NSF grant AST 87-14405 and a Fulbright fellowship (P. P.).

REFERENCES

Antonucci, R., & Miller, J. 1985, ApJ, 297, 621
Atherton, P. D., Reay, N. K., & Taylor, K. 1985, MNRAS, 216, 17P
Baldwin, J., Wilson, A. E., & Whittle, M. 1987, ApJ, 319, 84
Bushouse, H. A. 1987, ApJ, 320, 49
Cecil, G., Bland, J., & Tully, R. B. 1990, ApJ, 355, 70
Claussen, M. J., & Lo, K. Y. 1986, ApJ, 308, 592
Clements, E. D. 1981, MNRAS, 197, 731
Dahari, O. 1984, AJ, 89, 966
———. 1985, ApJS, 57, 643
Hernquist, L. 1989, Nature, 340, 687
Huntley, J. M. 1980, ApJ, 238, 524
Hutchings, J. B., & Campbell, B. 1983, Nature, 303, 584
Kallman, T., & Mushotzky, R. F. 1985, ApJ, 292, 49
Krabbe, A., Rotacine, V., Drapatz, S., & Genzel, R. 1990, in IAU Symposium 146, Dynamics of Galaxies and Molecular Cloud Distribution, ed. F. Combes (Dordrecht: Reidel), in press
Myers, S. T., & Scoville, N. Z. 1987, ApJ, 312, L39
Noguchi, M. 1988, A&A, 203, 259
Norman, C. A., & Scoville, N. Z. 1988, ApJ, 332, 124
Planesas, P., Gomez-Gonzales, J., & Martin-Pintado, J. 1989, A&A, 216, 1
Rand, R. J., & Kulkarni, S. R. 1990, ApJ, 349, L43
Roberts, W. W., Huntley, J. M., & van Albada, A. D. 1979, ApJ, 233, 67
Sandage, A. 1961, in The Hubble Atlas of Galaxies (Washington: Carnegie Institution of Washington)
Sandage, A., & Tammann, G. A. 1975, ApJ, 196, 313
Sanders, D. B., Soifer, B. T., Elias, J. H., Madore, B. F., Matthews, K., Neugebauer, G., & Scoville, N. Z. 1988, ApJ, 325, 74
Scoville, N. Z., & Good, J. C. 1989, ApJ, 339, 149
Scoville, N. Z., & Sanders, D. B. 1987, in Interstellar Processes, ed. D. J. Hollenbach & H. A. Thronson (Dordrecht: Reidel), p. 21
Scoville, N. Z., Matthews, K., Carico, D. P., & Sanders, D. B. 1988, ApJ, 327, L61
Scoville, N. Z., Young, J. S., and Lucy, L. B. 1983, ApJ, 270, 443
Telesco, C. M., Becklin, E. E., Wynn-Williams, C. G., & Harper, D. A. 1984, ApJ, 282, 427
Telesco, C. M., & Decher, R. 1988, ApJ, 334, 573
Thronson, H. A., Greenhouse, M. A., Johnson, P., Spillar, E., Hereld, M., & Majewski, S. N. 1989, ApJ, 343, 158
Ulvestad, J. S., Neff, S. G., & Wilson, A. S. 1987, AJ, 92, 22
Vogel, S. N., Kulkarni, S. R., & Scoville, N. Z. 1988, Nature, 334, 402
Wilson, A. S., & Ulvestad, J. S. 1982, ApJ, 263, 576
———. 1983, ApJ, 275, 8
———. 1987, ApJ, 319, 105
Wynn-Williams, C. G., Becklin, E. E., & Scoville, N. Z. 1985, ApJ, 297, 607
Young, J. S., & Sanders, D. B. 1986, ApJ, 302, 680